Results in Physics 9 (2018) 275–277

Contents lists available at ScienceDirect

Results in Physics

journal homepage: www.journals.elsevier.com/results-in-physics

# On the merging of optical and SAR satellite imagery for surface water mapping applications

Kel N. Markert [a,b,*], Farrukh Chishtie [c,d], Eric R. Anderson [a,b], David Saah [d,e,f], Robert E. Griffin [g]

[a] Earth System Science Center, The University of Alabama in Huntsville, United States
[b] SERVIR Science Coordination Office, NASA Marshall Space Flight Center, United States
[c] Department of Geospatial Information, Asian Disaster Preparedness Center, Thailand
[d] SERVIR-Mekong, Thailand
[e] Spatial Informatics Group, LLC, United States
[f] Geospatial Analysis Lab, University of San Francisco, United States
[g] Department of Atmospheric Science, The University of Alabama in Huntsville, United States

ARTICLE INFO

*Article history:*
Received 7 February 2018
Accepted 21 February 2018
Available online 24 February 2018

*Keywords:*
Optical imagery
SAR imagery
Data fusion
Surface water mapping
Applications

ABSTRACT

Optical and Synthetic Aperture Radar (SAR) imagery from satellite platforms provide a means to discretely map surface water; however, the application of the two data sources in tandem has been inhibited by inconsistent data availability, the distinct physical properties that optical and SAR instruments sense, and dissimilar data delivery platforms. In this paper, we describe a preliminary methodology for merging optical and SAR data into a common data space. We apply our approach over a portion of the Mekong Basin, a region with highly variable surface water cover and persistent cloud cover, for surface water applications requiring dense time series analysis. The methods include the derivation of a representative index from both sensors that transforms data from disparate physical units (reflectance and backscatter) to a comparable dimensionless space applying a consistent water extraction approach to both datasets. The merging of optical and SAR data allows for increased observations in cloud prone regions that can be used to gain additional insight into surface water dynamics or flood mapping applications. This preliminary methodology shows promise for a common optical-SAR water extraction; however, data ranges and thresholding values can vary depending on data source, yielding classification errors in the resulting surface water maps. We discuss some potential future approaches to address these inconsistencies.



## Introduction

Many studies have focused on the mapping of surface water using optical sensors (e.g. Landsat, Sentinel-2, and VIIRS) [1–3] and Synthetic Aperture Radar (SAR) sensors (e.g. Radarsat and Sentinel-1) [4,5]. Even with well-defined methods and readily available data from optical sensors for surface water mapping applications, its use is hindered by clouds that obscure surface observations; peak surface water extent during flood events can occur while there is cloud cover, resulting in data gaps and an inability to capture the accurate magnitude of such events. SAR data, on the other hand, can fill in gaps in optical data because SAR data can be acquired in all weather conditions and day or night. With the recent launch of Copernicus Sentinel-1 by the European Space Agency, SAR imagery has been applied more frequently for a variety of research and operational. This was due to data availability, high cost, and infrequent acquisitions plans of imagery. Even though the state of science for surface water extraction is mature for individual optical and SAR datasets, errors and uncertainties from individual algorithms can propagate into final merged thematic maps from two sources, resulting in uncertainties of the final representative map [6]. Few studies have explored the application of data fusion to produce consistent, harmonized surface water maps using similar techniques on both optical and SAR data tor to remedy limitations in both sensors.

In this paper, we introduce a method and preliminary results for merging optical and SAR with a focus of surface water mapping applications. This method is applied in a cloud-prone region, the Mekong basin in Southeast Asia. The Mekong Basin's climate is dominated by the Indian Monsoon resulting in a well-defined wet season with regular flooding. Due to the monsoon and the region being situated at a sub-tropical latitude and encircled by

* Corresponding author at: Earth System Science Center, The University of Alabama in Huntsville, 320 Sparkman Drive, Huntsville, AL 35805, United States.
*E-mail address:* km0033@uah.edu (K.N. Markert).

https://doi.org/10.1016/j.rinp.2018.02.054
2211-3797/

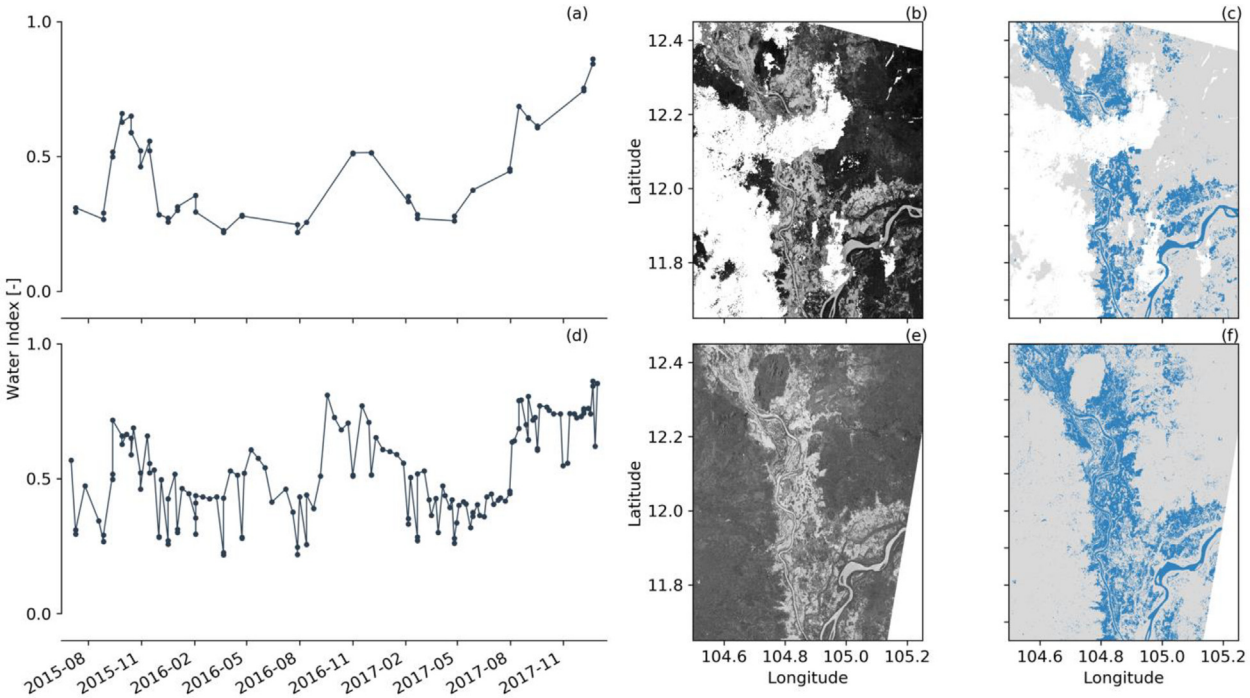


**Fig. 1.** Time series of water index values at 12.189°N, 104.823°E for (a) optical only and (d) combined optical-SAR. Imagery from the 17 Nov 2016 case display the calculated water index and extracted water mask for optical (b-c) and SAR (e-f) imagery. Brighter colors for the water index (b & e) indicate water pixels. The blue pixels indicate extracted water; and gray indicate land pixels for the water mask. White pixels in b, c, e, f are no data values arising from clouds or scene edges. (For interpretation of the references to colour in this figure legend, the reader is referred to the web version of this article.)

ocean, frequent cloud cover sometimes persists for lengthy periods of time. Cloud cover can impede the use of optical data for mapping of flood waters during flooding events, making the results from this study directly applicable to the region.

## Methods

Here we propose a method to harmonize optical and SAR data into a common data space. First, both datasets were processed into a representative index to highlight water features in a landscape. The Modified Normalized Difference Water Index (MNDWI) [7] was applied to top-of-atmosphere reflectance Landsat 8 imagery and rescaled between the maximum and minimum values for each scene, where higher values represent pixels more likely to be water. Automated surface water mapping algorithms using SAR imagery exist [8,9] which assume that signal sent by the satellite reflects off smooth surfaces (i.e. calm standing water) resulting in distiguishable low backscatter signals over water in all channels; however, the methods are not directly relatble to those using optical imagero produce a SAR water index analogous to an optical water index, Radiometrically Terrain Corrected (RTC) Sentinel-1 data was normalized by incidence angle using methods from Nguyen et al. [10] and then the absolute value of the sum across the VV and VH channels was calculated to highlight low backscatter values in each channel indicative of open water. Lastly, the SAR water index was rescaled to the maximum and minimum values and inverted so that values closer to 1 represent water similarly to the rescaled MNDWI optical imagery. The resulting data are both dimensionless with a range from 0 to 1 and are considered to be consistent and represent a common water index. Lastly, a simple thresholding approach was applied to the harmonized data to extract water bodies, in this case a threshold value of 0.55 was selected through visual interpretation of imagery. Resulting water pixels were filtered using the Height Above Nearest Drainage (HAND) topographic index [11] to remove detected water pixels from unrealistically hight elevations ultimately reducing errors caused by hill shadows [2]. The extracted water bodies were compared for a case study, 17 November 2016, at the confluence of the Mekong and Tonle Sap rivers where data from both sensors were collected. All data were processed and analyzed using Google Earth Engine [12].

## Results and conclusions

The process of integrating SAR imagery into the time series of Landsat acquisitions provides a denser time series for surface water mapping. Over the confluence of the Mekong-Tonle Sap Rivers between 1 July 2015 and 31 December 31, 2017, cloud-free observations from Landsat ranged from 1 to 79 samples at each pixel, with an average of 20 cloud-free observations. With the addition of Sentinel-1 data, the number of clear observations for individual pixels increased to a range of 94–172, with an average of 80 observations. Fig. 1 displays a time series of the calculated harmonized water index at 12.189°N, 104.823°E and the case study water extraction for 17 Nov 2016. The inclusion of SAR data decreases in variability with respect to time with a decreased coefficient of variability (CV) [13] of 0.31 for the optical and SAR series from 0.40 of only the optical series. The current methodology uses scene-based statistics to perform the rescaling, which results in differing frequencies of rescaled values between optical and SAR imagery. This can prove challenging for applying a static threshold for water extraction that can be applied across any image, a limitation that is observed in the resulting water maps for SAR data. When applying a single threshold to classify water across an entire dataset, we observe a slight over-estimation of surface water extent from SAR, especially for small water bodies, when compared to water masks derived from optical images alone (Fig. 1 c, f). This over-estimation may be due to speckling in the SAR imagery. Methods exists to despeckle SAR imagery [14,15], but they were not tested in this preliminary study.

The described methodology provides promising results in an effort to produce consistent optical and SAR surface water products and the prospects of creating consistent, dense surface water time series information for applications in cloud-prone regions. Further exploration is needed to refine the resulting water maps including, (1) implementing histogram matching to produce water index values that are more consistent across sensors and time, (2) applying atmospheric correction process to optical imagery, (3) applying speckle filtering of SAR images that results in a dataset still comparable to optical imagery, and (4) exploring the application of machine learning for surface water extraction to produce more dynamic extraction. After rigorous validation, the methods presented here and future work is planned to be used in a near real-time flood monitoring application in Southeast Asia.

## Acknowledgements

The authors would like to thank the data providers, NASA, USGS, EU Copernicus program, for making data freely available. This analysis contains modified Copernicus Sentinel data (2015-2017), processed by ESA. Also, a thanks to the Google Earth Engine team for allowing use of the platform for computing resources and data storage. We also thank Franz Meyer (University of Alaska Fairbanks/Alaska Satellite Facility) for interesting discussions and suggestions for this work. Lastly, the authors would like to thank the anonymous reviewers for their valuable comments contributing to the quality of the paper. Support for this work was provided through the joint US Agency for International Development (USAID) and National Aeronautics and Space Administration (NASA) initiative SERVIR, particularly through the NASA Applied Sciences Capacity Building Program, NASA Cooperative Agreement NNM11AA01A.

## References

[1] Chang Huang, Yun Chen, Jianping Wu, Linyi Li, Rui Liu. An evaluation of Suomi NPP-VIIRS data for surface water detection. Remote Sens Lett 2015;6(2):155–64. https://doi.org/10.1080/2150704X.2015.1017664.

[2] Donchyts G, Schellekens J, Winsemius H, Eisemann E, van de Giesen N. A 30 m resolution surface water mask including estimation of positional and thematic differences using landsat 8, SRTM and OpenStreetMap: a case study in the murray-darling basin, Australia. Remote Sens 2016;8(5):386. https://doi.org/10.3390/rs8050386.

[3] Pekel JF, Cottam A, Gorelick N, Belward AS. High-resolution mapping of global surface water and its long-term changes. Nature 2016;540:418–22. https://doi.org/10.1038/nature20584.

[4] Clement MA, Kilsby CG, Moore P. Multi-temporal synthetic aperture radar flood mapping using change detection. J Flood Risk Manage 2017. https://doi.org/10.1111/jfr3.12303.

[5] Pham-Duc B, Prigent C, Aires F. Surface water monitoring within Cambodia and the Vietnamese Mekong Delta over a year, with Sentinel-1 SAR observations. Water 2017;9:366. https://doi.org/10.3390/w9060366.

[6] Liu W, Gopal S, Woodcock CE. Uncertainty and confidence in land cover classification using a hybrid classifier approach. Photogramm. Eng. Rem. S. 2004;70(8):963–71. https://doi.org/10.14358/PERS.70.8.963.

[7] Xu H. Modification of normalized difference water index (NDWI) to enhance open water features in remotely sensed imagery. Int. J. Remote Sens. 2006;27:3025–33. https://doi.org/10.1080/01431160600589179.

[8] Westerhoff RS, Winsemius HC, Huizinga HJ, Brakenridge GR, Bishop C. Automated global water mapping based on wide-swath orbital synthetic-aperture radar. Hydrol. Earth Syst. Sc. 2013;17(2):651–63. https://doi.org/10.5194/hess-17-651-2013.

[9] Amitrano D, Di Martino G, Iodice A, Mitidieri F, Papa MN, Riccio D, Ruello G. Sentinel-1 for monitoring reservoirs: a performance analysis. Remote Sens. 2014;6(11):10676–93. https://doi.org/10.3390/rs61110676.

[10] Nguyen DB, Clauss K, Cao S, Naeimi V, Kuenzer C, Wagner W. Mapping Rice Seasonality in the Mekong Delta with Multi-Year Envisat ASAR WSM Data. Remote Sens. 2015;7:15868–93. https://doi.org/10.3390/rs71215808.

[11] Nobre AD, Cuartas LA, Hodnett M, Rennó CD, Rodrigues G, Silveira A, Waterloo M, Saleska S. Height Above the Nearest Drainage – a hydrologically relevant new terrain model. J. Hydrol. 2011;404:13–29. https://doi.org/10.1016/j.jhydrol.2011.03.051.

[12] Gorelick N, Hancher M, Dixon M, Ilyushchenko S, Thau S, Moore R. Google Earth Engine: Planetary-scale geospatial analysis for everyone ISSN 0034-4257. Remote Sens Environ 2017. https://doi.org/10.1016/j.rse.2017.06.031.

[13] Asfaw A, Simane B, Hassen A, Bantider A. Variability and time series trend analysis of rainfall and temperature in northcentral Ethiopia: A case study in Woleka sub-basin ISSN 2212-0947. Weather Clim Extremes 2017. https://doi.org/10.1016/j.wace.2017.12.002.

[14] Lee JS, Jurkevich L, Dewaele P, Wambacq P, Oosterlinck O. Speckle filtering of synthetic aperture radar images: A review. Remote Sensing Rev. 1994;8:313–40. https://doi.org/10.1080/02757259409532206.

[15] Zhu J, Wen J, Zhang Y. A new algorithm for SAR image despeckling using and enhanced Lee filter and median filter. In: 2013 6th International Congress on Image and Signal Processing (CISP).